Article:
Ettelaie, R orcid.org/0000-0002-6970-4650 and Lishchuk, SV (2015) Detachment force of particles from fluid droplets. Soft Matter, 11 (21). pp. 4251-4265. ISSN 1744-683X

https://doi.org/10.1039/C5SM00540J

Detachment force of particles from fluid droplets

Rammile Ettelaie[a] and Sergey V. Lishchuk*[b]

Received Xth XXXXXXXXXX 20XX, Accepted Xth XXXXXXXXX 20XX
First published on the web Xth XXXXXXXXXX 200X
DOI: 10.1039/b000000x

We calculate the deformation of a spherical droplet, resulting from the application of a pair of opposite forces to particles located diametrically opposite at the two ends of the droplet. The free-energy analysis is used to calculate the force–distance curves for the generated restoring forces, arising from the displacement of the particles relative to each other. While the logarithmic dependence of the "de Gennes–Hooke" constant on the particle to droplet size ratio, ν, is rather well known in the limit of very small ν, we find that for more realistic particle to droplet size ratios, *i.e.* $\nu = 0.001$ to 0.01, the additional constant terms of $O(1)$ constitute a significant correction to previously reported results. We derive the restoring force constant to be $2\pi\gamma[0.5 - \ln(\nu/2)]^{-1}$, in perfect agreement with the exact semi-numerical analysis of the same problem. The deviation from the linear force–displacement behaviour, occurring close to the point of detachment, is also investigated. A study of the energy dissipated shows it to be an increasingly dominant component of the work done during the detachment of the particles, as ν decreases. This indicates the existence of a significantly higher energy barrier to desorption of very small particles, compared to the one suggested by their adsorption energy alone. The influence of the line tension on the detachment force is also considered. It is shown that where line tension is important, the contact angle is no longer a constant but instead alters with the displacement of the particles from their equilibrium positions.

1 Introduction

The behaviour of small particles trapped at liquid-liquid or liquid-gas interfaces continues to be an area of great interest both from an academic point of view, as well as for its importance in many industrial applications. The adsorption of hydrophobic or partially hydrophobic particles to the surface of bubbles during the froth flotation process is often considered to be the most widespread technique in recovery and separation of ore minerals in mining and related industries[1,2]. The crucial role played by particles adsorbed at surfaces, in destabilisation of bubbles has similarly been well known and frequently used to prevent foaming[3,4], as for example in defoaming of liquids used in air-conditioners and cooling systems. Interestingly, it is now also well recognised that particles with appropriate surface chemistries, and hence contact angles, can stabilise bubbles and emulsion droplets against many different modes of colloidal instability, including coalescence, Ostwald ripening and disproportionation[5–8]. Indeed, the adsorption of nanoparticles onto the surface of microbubbles remains one of the very few methods that seem to be genuinely able to arrest the disproportionation process in such systems and ensure the long term stability for these very small bubbles[9]. The adsorption energy for a particle adsorbed at a liquid-air interface is easily shown to be[7,10]

$$E_{ad} = \pi\gamma a^2(1-\cos\theta)^2 \qquad (1)$$

where γ is the surface tension, a is the radius of the particle, and θ is the contact angle between the liquid and a solid substrate comprising of the same material as that for the particle. More precisely, the energy difference as given by Eq. (1) refers to the energy of a particle that has been fully displaced from the interface into the bulk phase, as measured relative to its energy when setting at equilibrium at the surface. The particle displacement here is assumed to be into the more dense liquid phase, *i.e.* the one into which the contact angle θ is traditionally measured. If the particle is moved into the opposite phase, then the factor $(1-\cos\theta)$ in Eq. (1) needs to be replaced with $(1+\cos\theta)$. The result in equation (1) also takes into account any interfacial energy associated with the creation of an additional circular contact area between the two bulk phases, which originally would have been occupied by the particle when at the interface. Even for a small nanoparticle of radius $a = 10\,\text{nm}$, the adsorption energy can be several tens of thousands of k_BT. Thus, particles, once adsorbed, are rather difficult to displace from the interfaces. It is this property which makes the particles such a good colloidal stabilisers of emulsions and bubbles. In a similar manner, particles accumulating at the interfaces between two phases, formed during the demixing of two fluids through spinodal decomposition, can arrest the phase separation at some intermediate stage during the process. This gives rise to the so called bicontinuous

[a] *Food Colloids Group, School of Food Science and Nutrition, University of Leeds, Leeds LS2 9JT, United Kingdom.*
[b] *Department of Mathematics, University of Leicester, Leicester LE1 7RH, United Kingdom.*

interfacially jammed emulsion gel (bijel) systems[11–14], first predicted theoretically by Cates and co-workers[15].

While the adhesion of particles to the surface seems irreversible in many situations, it is nonetheless possible to cause desorption of these through the application of a suitable external field. For example magnetic or electrically polarisable particles are shown to detach from the interfaces in the presence of strong enough magnetic or electrical fields[16–18]. Similarly, a higher density of particles relative to the surrounding liquid medium may be sufficient to detach the particles from the bubbles, as the bubbles try to rise and the particles are pulled down by the gravity[19]. Detachment of the particles from the surface of such Pickering stabilised bubbles or droplets normally leads to the breakup of the foam or the emulsion system. The triggered destabilisation of the emulsions has many potential applications, as for example in the targeted release of drugs. Development of such vehicles for controlled delivery could benefit from a clearer understanding of the nature and magnitude of restoring forces that result from the displacement of a particle, when it is disturbed from its equilibrium position on an interface. Control of the particle adsorption or detachment is important in liquid marbles which have promising applications in micro-chemical and bioreactors[20–22] and tuning droplet impact dynamics[23].

On the experimental side, several studies involving atomic force microscopy and micro-force balance have provided a detail account of the forces that result during the approach, subsequent attachment, and finally the detachment of particles from the surface of bubble[24–32]. Close to the surfaces of bubbles, and prior to the attachment of the particle, the forces involved are a combination of the well-known colloidal interactions, namely van der Waals, electrostatic and hydrophobic forces[26,33]. Where the surface of particles or bubble is covered by macromolecules, additional interactions involving steric repulsion, as well as bridging and depletion attractions, may also be present[34–36]. At the point of attachment, there is a discontinuous jump in the value of measured force. From this point onward the variation of the force with displacement is largely governed by the interfacial tensions between the two surrounding fluids (*e.g.* air-water or oil-water) and the fluids and the particle. In particular, the experimental results suggest that in the majority of cases the restoring forces generated as a result of the displacement of a particle trapped on the surface of a bubble or droplet, away from its equilibrium position, varies almost in a linear fashion with the displacement of the particle[30]. This linear Hookean type variation, first suggested by Joanny and de Gennes[37,38], continues to distances almost up to the point where the particle becomes detached from the droplet, *i.e.* where the force reaches its maximum value, shortly prior to the particle leaving the interface. However, determining the range of validity of "de Gennes-Hooke's" law analytically is an interesting problem that is considered here.

The theoretical treatment of the detachment of the particles from fluid interfaces has largely focused on situations involving planar interfaces, where the gravitational, and in some cases also the buoyancy forces, are included[39–50]. Such situations are of course what one encounters in problems relating to the process of froth flotation. These types of analysis provide limits on the size of particles that can be floated on the interface and also the maximum detachment forces necessary to pull the particles out and away from the surface. Huh and Scriven[51] provide tabulated numerical data for the shape of an equilibrium fluid that extends far outwards from a circular line of contact away from an immersed cylinder, given as a function of radius of the contact circle, contact angle, surface tension and density difference across the interface. Analytical results for the same problem have been obtained by Rapacchietta and Neumann[43] in the limit of small Bond numbers (ratio of gravity forces to capillary ones). These authors considered forces acting on the particle during the detachment process and proposed the particle/interface aggregate stability criteria based on the work of detachment of the particle from the interface. The detachment work of a small sphere from a surface was also considered analytically by Pitois and Chateau[47,48] making use of Derjaguin approximation. Comparing their analytical and experimental data, the importance of the contact angle hysteresis for the detachment work was highlighted in this work. Kowalczuk and Drzymala[49], using equations derived by Scheludko *et al.*[41], show how experiments involving attachment and detachment of particles to a liquid interface could be used to determine the static, attachment and detachment contact angles using a Washburn-type technique. Indeed, pulling a sphere through the liquid interface is the basis for measuring the surface tension and contact angle of liquids on spherical surfaces in a technique often referred to as sphere tensiometry[40,44,46,52–54]. O'Brien[45], working in the low Bond number limit (Bo $\ll 1$), has proved that the restoring force resulting from the displacement of the particle from its equilibrium position on the interface can satisfactorily be described as a linear function of the distance, in a similar manner to the Hooke's law as had been anticipated by Joanny and de Gennes[37].

The inclusion of gravity in all of the calculations mentioned above, even those involving small Bo numbers, and in particular for the fluid phase, is rather crucial in allowing such theoretical analysis to be performed. The boundary condition assuming a flat interface at distances far from the contact line, will fail to provide an analytical solution in the complete absence of gravity. The situation is best demonstrated by considering an air–water interface where the displacement of the particle into the air causes the distortion of the interface. The rise of the liquid pulled up with the particle involves additional gravitational energy. For example, for a rather simple case involving a rectangular slab held partially immersed in a liquid,

the height to which the fluid will rise next to the slab is found to be $h = \sqrt{(2\gamma/\rho g)(1-\sin\theta)}$ when $\theta \leq \pi/2$, where g is the gravitational strength and ρ is the density of the fluid[55]. In the absence of gravity where $\rho g \to 0$ we have $h \to \infty$. In the same manner, the distance away from the particle to which the distortion of the interface extends also diverges in the absence of gravity. This holds true for the slab problem[55] above, as well as cylindrical objects[42,51] and cases involving spherical particles[41,43]. Clearly this is expected, since in absence of the gravitational energy associated with the distortion of the liquid interface, the whole bulk of the liquid will simply move up with the particle such that the position of the particle relative to the liquid interface remains the same as its equilibrium value.

In problems involving the displacement of particles from the surface of bubbles or droplets dispersed throughout a medium, as for example in Pickering emulsions, inclusion of gravity is neither appropriate nor relevant. It would be incorrect to attribute a gravitational energy to any distortion of the interface in these circumstances. It is clear then, that in order to be able to make progress with the theoretical calculations one has to either apply an equal but opposite counter force (to the one acting on the particle) to some part of the particle-droplet system, or alternatively impose some constraint to prevent the displacement of the system as a whole. One possible approach would be to apply a pair of opposite forces of magnitude F to the particle and the centre of mass of the droplet. In a real situation such a counter force may arise from the drag experienced by the droplet, given by $F \sim 6\pi\eta Ru$ if the spherical shape of the droplet is not severely distorted. Here, u is the velocity of the system under the influence of the external force applied to the particle, R is the radius of the droplet, and η the viscosity of the dispersion medium. Alternatively, one may impose the "effective" constraint that the liquid continues to fully wet the surface of the container in which it resides, as the particles are slowly displaced and eventually become detached from the air–liquid interface. This is the approach adopted by Davies *et al.*[50] where also the volume of the liquid phase is kept constant. In their study, the detachment energy for a variety of particles with different spheroidal shapes, including oblate and prolate spheroids, is numerically calculated using a suitable lattice Boltzmann simulation scheme. All else being the same, it is found that the detachment energy can be expressed as a function of the particle aspect ratio and the height of the centre of mass of the particle above the fluid interface at equilibrium[50]. These results are used in a latter study by the same authors to consider the impact on an ensemble of such spheroid particles accumulated at a liquid interface[56]. Note that the requirement for the container walls to be fully wetting, together with constant volume of the liquid phase, ensure that the air–water interface will once again be a flat one at distances far from the particle, even when no gravity is present.

Yet, a further possibility in choosing a suitable constraint is the one employed by Guzowski *et al.*[57]. There, the centre of mass of the droplet (or the droplet+particle system) is restrained, remaining fixed throughout the calculations irrespective of the distortion of the droplet shape. The actual problem considered in this work consisted of a particle which sat on the surface of a sessile droplet, to which a force F was then applied. As such, the calculations of Guzowski *et al.* involved two distinct contact angles; one between the particle and the droplet and the other between the droplet and the substrate. They derive an interesting, and in principle rather general, formalism for solving this problem. They argue that the quantity $\varepsilon = F/(\gamma R)$ (i.e. the ratio of the pressure perturbation due to force F applied to the particle to the excess Laplace pressure inside the droplet) remains small in almost all practical situations. Thus, the equations describing the disturbance of the interface, the shift in the position of the particle and the values of the Lagrange multipliers, associated with constraints imposed on total volume and fixed position of the centre of mass of the droplet, can all be linearised in this small parameter ε. The linear nature of the equations allows the problem to be formulated in terms of Green's functions, with the latter giving the response of the interface to a unit point force applied at any desired position on the surface of the droplet. Using the method of images, Guzowski *et al.*[57] derive explicit expressions for their Green's functions, in the special symmetrical case where the contact angle between droplet and substrate is 90°. In principle then, the response of the interface to the application of a force to a small but finite sized particle, can be obtained by replacing this particle with a series of appropriate point forces acting along an imaginary surface passing through the particle. However, in their work Guzowski *et al.* mainly focus on cases involving very small particles ($\nu \equiv a/R \ll 1$) where, at least for the interfacial disturbance far from the particle (distances much larger than a) it suffices to treat the particle as a point source. The results of this approach are evaluated against "exact" numerical (finite-elements) and semi-analytical solutions (solving the non-linearised equations in special cases, but with boundary conditions having to be fitted numerically) and found to provide a good level of agreement.

In the current study we consider a droplet (or bubble) having two particles adsorbed at its surface placed diametrically opposite each other. The symmetry of the problem and hence the mathematical formulation is identical to one of the earlier papers on an axisymmetric capillary bridge by Orr, Scriven and Rivas[58]. We apply equal but opposite forces to each particle as is shown schematically in Figure 1. The symmetrical nature of the problem, considered in this way, provides significant simplifications allowing us to obtain exact analytical expressions for the distortion of the spherical bubble, and hence the force vs displacement curves as the particles are pulled away from each other. In the limit where the radius of

droplet $R \to \infty$, the current problem becomes identical to the one studied by Davies *et al.* for their spherical particle case[50]. Our problem is identical to that considered by Guzowski *et al.* when the contact angle between their sessile drop and the substrate is 90° and the particle is located at the apex of the drop. We attempt to extend their calculations to provide analytical expressions for the distortion in the shape of the droplets in the small v limit. While Guzowski *et al.* also considered simplifications to their more general analysis for small particle cases[57], here our analytical expressions for the distortion of the shape of the droplets, as well as force vs particle displacement, are obtained without resort to such a linearisation in the force term. This allows for a very accurate description of the interfacial distortion and the force displacement relation right up to the point of the detachment of the particle, and even at distances very close to the particle (i.e. $< a$). Thus, one is able to assess the range of the validity of the "Hooke-de Gennes" law and the linearity of the force displacement relationship. Furthermore, Guzowski *et al.* showed that to the leading term, the dependence of the "compliance constant" on the size ratio of the particle to the droplet, v, is logarithmic[57]. While for very small values of v this term alone suffices in determining the value of the compliance, we note that typical size ratio for Pickering stabilised emulsions in practice lie in the range between 0.001 and 0.01 (*e.g.* nanoparticles of $a \sim 5$ nm stabilising droplets of $R \sim 1\,\mu$m). These values of v are small, but nonetheless $-\ln v \sim 4.6$ to 6.9. This means that the presence of a constant term of $\sim O(1)$ can constitute a major correction to the actual value of the "compliance constant", which can only be ignored in problems where the size ratio is unrealistically small. It is one of our aims in this work to calculate a more accurate value for the compliance constant that should remain valid for these small but nonetheless more practical values of v.

The paper is organised as follows. The details of our model system are described in Section 2. Section 3 presents, without derivation, the key result of the present work: *i.e.* the analytical expression for dependence between the force and the displacement of the particles in the limit of small ratio of particle to droplet sizes. The rest of the paper details the derivation of this result and its consequences. The solution of the variational problem corresponding to the model of Section 2 is presented in Section 4 leading to exact "semi-analytical" results for the problem, valid for any particle size. In Section 5, the small particle to the bubble size ratio limit is explored to provide analytical expression for the distortion of the droplet surface and the displacement of the particles on each side of the droplet, resulting from the application of equal but opposite forces F to the particles. In Section 6, using our force vs displacement graphs we consider the dissipation of the energy that arises from the detachment of a particle from the interface. Finally, we discuss the effect of line tension in Section 7.

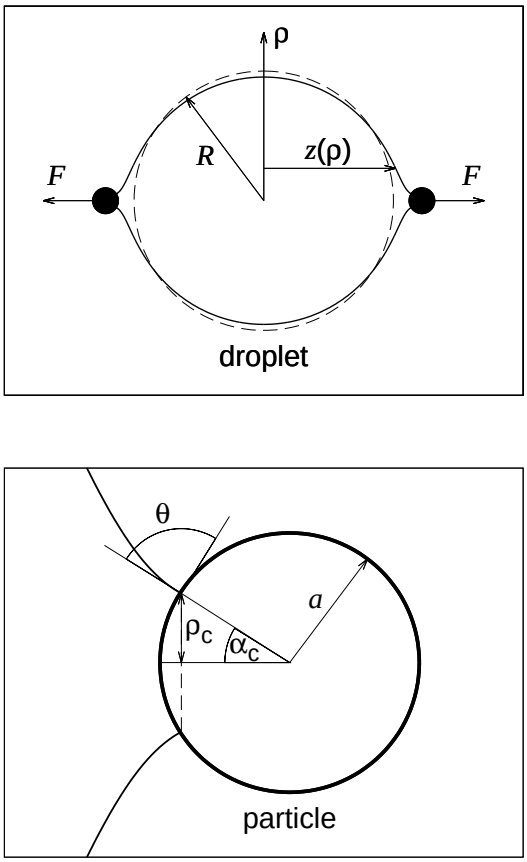

Fig. 1 The geometry of the system.

2 Model

The geometry of our system is shown in Figure 1. We consider a droplet of incompressible fluid 1 immersed in fluid 2. Due to surface tension between the two fluids, the droplet in equilibrium is spherical with radius R, which is determined by the volume V_0 of the droplet given by

$$V_0 = \frac{4\pi}{3}R^3. \tag{2}$$

In order to overcome the problem of having a net zero force on the droplet–particle system we use two identical solid particles of radius a adsorbed at the opposite ends of the droplet. The equilibrium contact angle between the fluid interface and the flat surface, θ, is determined by Young's equation

$$\theta = \arccos\left(\frac{\gamma_{1p} - \gamma_{2p}}{\gamma}\right), \tag{3}$$

where γ_{1p} and γ_{2p} are surface tensions of the surface of the

particles in contact with fluids 1 and 2, respectively. The resulting system is axially symmetric. We take the denser continuous fluid phase to be phase 2 here, with the fluid 1 then comprising the body of the droplet. As such, the contact angle is then conventionally measured as the one considered into the phase 2.

We apply opposite forces, $\mathbf{F}$ and $-\mathbf{F}$, on both particles, acting along the axis of symmetry of the system. Our aim is to establish the positions of the centre of the particles, $\mathbf{r}_1$ and $\mathbf{r}_2$, as the functions of the applied force of magnitude F. Under applied force the system will remain symmetric, so that $r_1 = -r_2 \equiv r$, where r is the distance of the particle centre from the centre of mass of the fluid droplet.

We can write the magnitude of the external force applied to the particles as the derivative of the free energy of the system, $\mathscr{F}$, with respect to distance $2r$ between them:

$$F = \frac{d\mathscr{F}}{d(2r)}. \tag{4}$$

Free energy of the system is determined by presence of the interfaces and can be written as

$$\mathscr{F} = \gamma S_{12} + \gamma_{1p} S_{1p} + \gamma_{2p} S_{2p}, \tag{5}$$

where the quantities S denote areas between different constituents, indicated by subscripts 1, 2 and p, corresponding to fluids 1 and 2 and the particles, respectively. Similarly, the subscript for each γ indicates the interfacial tension between the indicated phases. We neglect line tension for the moment.

Generally, the free energy of the system is the functional of the shape of the droplet. The equilibrium shape of the droplet at given particle positions can be obtained by minimising the free energy of the system (5) with respect to possible droplet shape, with the additional constraint of constant volume of the droplet,

$$V = V_0, \tag{6}$$

where V_0 is given by Eq. (2). This condition arises due to incompressibility of the droplet fluid.

3 Displacement–force diagram in small-particle limit

This section presents, without derivation, the key result of the present work: the analytical expression for dependence between the force F and the displacement of the particles Δr in the limit of small ratio of particle to droplet sizes. It is given parametrically by the formulas

$$F(\kappa) = \pi\gamma a \mu \tag{7}$$

and

$$\Delta r(\kappa) = a\left\{\sqrt{1-\kappa^2} - \frac{\mu}{4}\left[1 + 2\ln\frac{(\kappa+\xi)a}{4R}\right]\right\}, \tag{8}$$

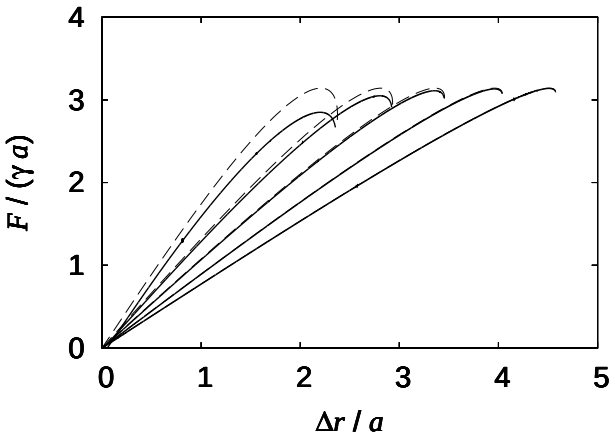

Fig. 2 Dependence of force upon the position of the particles at $\theta = 90^\circ$. Solid curves are calculated numerically and correspond to $\nu = 0.1, 0.03, 0.01, 0.003, 0.001$ (from left to right). Dashed curves correspond to the small-particle limit, Eq. (12).

where

$$\xi = \sqrt{\kappa^2 - \frac{\mu^2}{4}}, \tag{9}$$

$$\mu = 2\kappa\left(\sqrt{1-\kappa^2}\sin\theta - \kappa\cos\theta\right), \tag{10}$$

and the parameter κ changes between $\kappa_{\min}$ and 1, where $\kappa_{\min}$ is the solution of transcendental equation

$$\left(\frac{d\Delta r(\kappa)}{d\kappa}\right)_{\kappa=\kappa_{\min}} = 0, \tag{11}$$

with $\Delta r(\kappa)$ being given by Eq. (8).

In the case of 90° contact angle, the displacement can be expressed explicitly as a function of the force:

$$\frac{\Delta r}{a} = \sqrt{\frac{1\mp\Phi}{2}} - \frac{F}{2\pi\gamma a}\left\{\frac{1}{2} + \ln\left[\frac{a}{8R}\left(1\pm\Phi+\sqrt{2(1\pm\Phi)}\right)\right]\right\}, \tag{12}$$

where

$$\Phi = \sqrt{1-\left(\frac{F}{\pi\gamma a}\right)^2}. \tag{13}$$

The derivation of the above formulas and their consequences is given in the rest of the paper. Figure 2 demonstrates the accuracy of these formulas in comparison with the full numerical solution, described in Subsection 4.4, at different values of particle to droplet size ratios, as do Figures 3, 5–9 and 11 further.

4 Free-energy analysis

In this Section the free-energy analysis is performed for the model described in Section 2. We obtain the exact expressions for the shape and volume of the droplet, as well as the free energy of the system as functions of three parameters which characterise the size of the droplet, its deformation and the radius of the contact circle. Following this we solve numerically for the values of these parameters which minimise the free energy of the system under the constraint of constant volume of the droplet, given by Eq. (6), and use the results to calculate the detachment force and other properties of the system.

4.1 Droplet shape.

Minimisation of the free energy of the system under the constraint of fixed volume constitutes a variational problem with variable end points. Different equivalent methods exist for solving this class of variational problems, which are discussed, for example, by Bolza[59]. We adopt the method in which the variational problem is decomposed into two problems[60]. First we consider the variations which leave the end points fixed (which physically corresponds to pinned contact line). After that, finding the extremal satisfying boundary conditions reduces to an algebraic problem, which is simpler than considering from the beginning the full variation including the end points.

In accordance with the above, we first determine the class of the shapes of the fluid droplet which minimise the contribution to free energy due to the presence of the fluid interface only. This contribution is proportional to the area of the fluid interface, $\mathscr{F}_{12} = \gamma S_{12}$, so the problem is equivalent to minimising the area S_{12} at constant volume of the droplet. The result will depend on the parameters which will be later determined by minimising the total free energy of the system.

It is convenient in our study to describe the droplet shape by the function $z \equiv z(\rho)$, where the cylindrical polar coordinates ρ and z are depicted in Figure 1. Henceforth we shall omit the argument ρ for brevity when referring to z. The element of the arc length corresponding to the increment $d\rho$ is

$$dl = \sqrt{1+z'^2}d\rho, \tag{14}$$

where prime denotes derivative with respect to ρ. The corresponding elements of the surface area and the volume are given by

$$dS = 2\pi\rho dl \tag{15}$$

and

$$dV = 2\pi\rho z d\rho. \tag{16}$$

The function to be minimised is

$$\mathscr{S} = S_{12} + \frac{2}{\rho_0}V. \tag{17}$$

Here

$$S_{12} = \int dS \tag{18}$$

is the area of the fluid interface and

$$V = \int dV \tag{19}$$

is the volume of the droplet, and $(2/\rho_0)$ is Lagrange multiplier associated with the fixed volume of the droplet. The function (17) can be represented in the form

$$\mathscr{S} = \int L d\rho, \tag{20}$$

with the integrand function given by

$$L = 2\pi\rho\left(\sqrt{1+z'^2} + \frac{2z}{\rho_0}\right). \tag{21}$$

The corresponding Euler-Lagrange equation,

$$\frac{\delta L}{\delta z} = \frac{\partial L}{\partial z} - \frac{d}{d\rho}\frac{\partial L}{\partial z'} = 0, \tag{22}$$

then becomes

$$\rho z'' + \left(1+z'^2\right)\left(z' - \frac{2\rho}{\rho_0}\sqrt{1+z'^2}\right) = 0. \tag{23}$$

The solution to this equation is

$$z' = -\frac{\frac{1}{2}c\rho_0^2 + \rho^2}{\sqrt{\rho_0^2\rho^2 - \left(\frac{1}{2}c\rho_0^2 + \rho^2\right)^2}}, \tag{24}$$

where c is integration constant. Due to the symmetric nature of the problem, the condition $z' = -\infty$ gives the maximum and minimum radii of the cross-section of the droplet:

$$\rho_+ = \sqrt{\frac{1-c+\sqrt{1-2c}}{2}}\rho_0. \tag{25}$$

$$\rho_- = \sqrt{\frac{1-c-\sqrt{1-2c}}{2}}\rho_0. \tag{26}$$

To obtain the formula for the droplet shape, we integrate z' to yield

$$z = \int_{\rho_+}^{\rho} z' d\rho = \int_{\rho}^{\rho_+} \frac{\left(\frac{1}{2}c\rho_0^2 + \rho^2\right)d\rho}{\sqrt{(\rho_+^2 - \rho^2)(\rho^2 - \rho_-^2)}} \tag{27}$$

The resulting shape is the so called unduloid[58,61] described by formula

$$z = \rho_+ E(\varphi, k) + \frac{c\rho_0^2}{2\rho_+}F(\varphi, k), \tag{28}$$

where $F(\varphi,k)$ and $E(\varphi,k)$ are incomplete elliptic integrals of first and second kind, respectively, and

$$\sin\varphi = \sqrt{\frac{\rho_+^2-\rho^2}{\rho_+^2-\rho_-^2}}. \tag{29}$$

and

$$k = \sqrt{1-\frac{\rho_-^2}{\rho_+^2}}. \tag{30}$$

In cases $c>0$ and $c<0$ Eq. (28) describes, respectively, unduloids and nodoids, which are members of the family of constant mean curvature surfaces[58,61]. They correspond to the detachment of the particles in the outward and inward direction with respect to droplet. We shall henceforth consider the case when the particles detach in the outward direction ($c>0$). Note that at $c=0$ the shape described by Eq. (28) reduces to a spherical one,

$$\lim_{c\to 0} z = \sqrt{\rho_0^2-\rho^2}. \tag{31}$$

4.2 Free energy.

In this subsection we obtain the explicit formula for the free energy of the system. For this, we need the expressions for the contact areas between different constituent phases.

Due to the symmetry of the problem, the surface of the droplet contacts the particles at circular lines. We denote their radii as ρ_c. Then the interfacial areas can be represented as

$$S_{1p} = 2\left[2\pi a\left(a-\sqrt{a^2-\rho_c^2}\right)\right], \tag{32}$$

$$S_{2p} = 2\left[2\pi a\left(a+\sqrt{a^2-\rho_c^2}\right)\right], \tag{33}$$

$$S_{12} = 2\cdot\int_{\rho_c}^{\rho_+}\frac{2\pi\rho_0\rho^2 d\rho}{\sqrt{(\rho_+^2-\rho^2)(\rho^2-\rho_-^2)}} = \\ = 2\left[2\pi\rho_+\rho_0 E(\varphi_c,k)\right] \tag{34}$$

with

$$\sin\varphi_c = \sqrt{\frac{\rho_+^2-\rho_c^2}{\rho_+^2-\rho_-^2}}. \tag{35}$$

Note that in the case of a spherical droplet ($c=0$) the surface area of the fluid–fluid interface reduces to that for a spherical zone:

$$\lim_{c\to 0} S_{io} = 4\pi\rho_0\sqrt{\rho_0^2-\rho_c^2}. \tag{36}$$

As a result, the free energy of the system, up to a constant term, is

$$\mathscr{F} = 4\pi\gamma\left[\rho_+\rho_0 E(\varphi_c,k) - a\sqrt{a^2-\rho_c^2}\cos\theta\right]. \tag{37}$$

4.3 Droplet volume.

In this subsection we obtain the expression for the volume of the droplet which corresponds to the shape described by Eq. (28). We shall impose the constraint of constant volume of the droplet, given by Eq. (6), when we come to minimise the free energy of the system.

First we consider the case when the angle

$$\alpha_c = \arcsin\frac{\rho_c}{a}, \tag{38}$$

as depicted in Figure 1, satisfies the condition

$$\alpha_c \le \frac{\pi}{2}. \tag{39}$$

In this case the volume of the droplet can be written as

$$V = V_{\rho<\rho_c} + V_{\rho>\rho_c}, \tag{40}$$

where

$$V_{\rho<\rho_c} = 2\left(2\pi\int_0^{\rho_c}\rho z d\rho\right) \tag{41}$$

and

$$V_{\rho>\rho_c} = 2\left(2\pi\int_{\rho_c}^{\rho_+}\rho z d\rho\right). \tag{42}$$

In the integral (41), z is the position of the surface of the particles:

$$z = r - \sqrt{a^2-\rho^2}. \tag{43}$$

The integration yields

$$V_{\rho<\rho_c} = \frac{4\pi}{3}\left\{\frac{3}{2}\rho_c^2 r - \left[a^3-(a^2-\rho_c^2)^{3/2}\right]\right\}. \tag{44}$$

In the integral (42), z is the position of the fluid-fluid interface. The integration yields

$$V_{\rho>\rho_c} = \frac{4\pi}{3}\left\{\rho_+\left[\rho_+^2+\rho_-^2-\frac{3}{2}\rho_c^2+\frac{3}{4}c\rho_0^2\right]E(\varphi_c,k) \right. \\ -\left[\frac{\rho_-^2\rho_+}{2}+\frac{3}{4}\frac{c\rho_0^2\rho_c^2}{\rho_+}\right]F(\varphi_c,k) \\ \left. +\frac{\rho_c}{2}\sqrt{(\rho_+^2-\rho_c^2)(\rho_c^2-\rho_-^2)}\right\}. \tag{45}$$

Note, in the case of an undeformed droplet ($c=0$) we have the volume of relative complement of cylinder of radius ρ_c in sphere of radius ρ_0 (spherical ring):

$$\lim_{c\to 0} V_{\rho>\rho_c} = \frac{4\pi}{3}(\rho_0^2-\rho_c^2)^{3/2}. \tag{46}$$

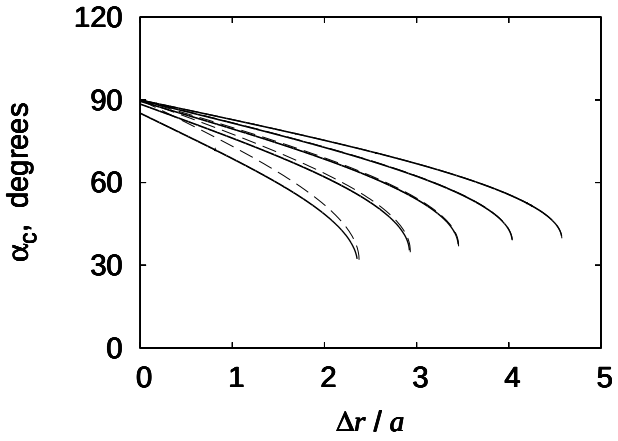

Fig. 3 Dependence of the angle α_c, defined by Eq. (38) and depicted in Figure 1, upon the position of the particles at $\theta = 90^\circ$. Solid curves are calculated numerically and correspond to $v = 0.1, 0.03, 0.01, 0.003, 0.001$ (from left to right). Dashed curves correspond to the small-particle limit, Eq. (69).

As a result, the volume of the droplet is given by formula

$$V = \frac{4\pi}{3}\left\{\left[\left(1-\frac{c}{4}\right)\rho_0^2 - \frac{3}{2}\rho_c^2\right]\rho_+ E(\varphi_c,k) - \left[\frac{\rho_-^2\rho_+}{2} + \frac{3}{4}\frac{c\rho_0^2\rho_c^2}{\rho_+}\right]F(\varphi_c,k) + \frac{\rho_c}{2}\sqrt{(\rho_+^2-\rho_c^2)(\rho_c^2-\rho_-^2)} + \frac{3}{2}\rho_c^2 r - \left[a^3 - (a^2-\rho_c^2)^{3/2}\right]\right\}. \quad (47)$$

Finally, in the case $\alpha_c > \pi/2$, *i. e.* opposite situation to that defined by Eq. (39), the volume of two spherical rings with sphere radius a and cylindrical hole radius ρ_c,

$$\frac{4\pi}{3}\left(a^2-\rho_c^2\right)^{3/2}, \quad (48)$$

which corresponds to the volume at $\rho > \rho_c$ which lies inside the particles and therefore should be subtracted from the total volume, Eq. (47), to yield the actual volume of the fluid droplet. This is particularly important when the size of particles becomes comparable to that of the droplet.

4.4 Numerical solution.

We have obtained the exact expressions for the shape, Eq. (28), and volume, Eq. (47), of the droplet, as well as the free energy of the system, Eq. (37), as functions of the parameters ρ_0, c, and ρ_c, which characterise size and deformation of the droplet and radius of the contact circle, respectively. The actual values

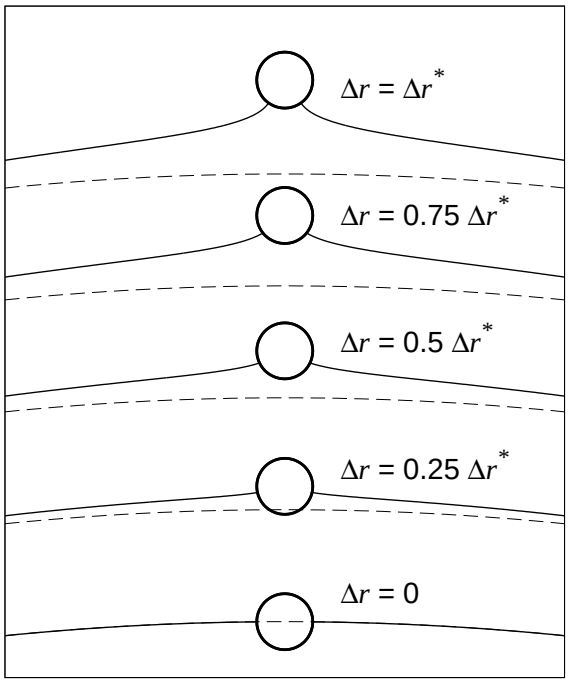

Fig. 4 Shapes of the droplet surface at different positions of the particle, calculated for $v = 0.01$ and $\theta = 90^\circ$. Dashed lines correspond to equilibrium shape of the droplet. The top figure shows particle position which corresponds to maximum force for which the particle still remains attached to the interface.

of these parameters are those that minimise the free energy of the system. The minimisation should be undertaken under two conditions. First, the volume of incompressible fluid in the droplet should be constant, *i. e.* Eq. (6). Second, the interface should contact particle at circle of radius ρ_c, which can be cast as equality of the value $z(\rho_c)$, calculated using Eq. (28) for the droplet shape, to the value of z calculated using Eq. (43) for the shape of the particle.

In order to calculate the force required to detach the particle from the droplet we proceed as follows. We fix the value of particle displacement Δr defined as

$$\Delta r = r - R \quad (49)$$

and solve numerically for the values of the parameters ρ_0, c, and ρ_c, which minimise free energy under the conditions given above. Repeating this procedure for different values of Δr we obtain free energy of the system, $\mathscr{F}$, as a function of particle displacement. Then we use numerical differentiation to calculate the force as a function of particle position according to

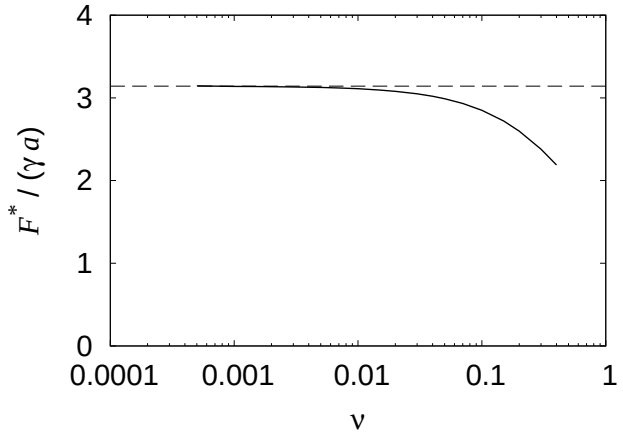

Fig. 5 Dependence of the detachment force with ν, at $\theta = 90^\circ$. Solid curve is calculated numerically. Dashed curve corresponds to the small-particle limit, Eq. (70).

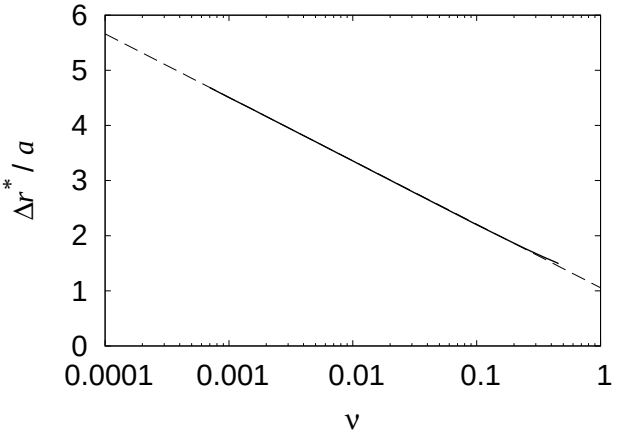

Fig. 6 Dependence of the particle position, corresponding to the point where the maximum force occurs, with ν at $\theta = 90^\circ$. Solid curve is calculated numerically. Dashed curve corresponds to the small-particle limit, Eq. (71).

Eq. (4). In force-measuring experiments the maximum of this function corresponds to the detachment force.

We start by considering the case of 90 degree contact angle. Figures 2 and Figure 3 show the dependence of the force, calculated using Eq. (4), and the angle α_c, defined by Eq. (38), upon particle displacement, at different values of the ratio of particle to droplet sizes, denoted as

$$\nu \equiv \frac{a}{R}. \tag{50}$$

The resulting shapes for the droplet surface at different values of the particle displacement, calculated at $\nu = 0.01$, are shown at Figure 4. The force–displacement dependence shown in Figure 2 is similar to the experimental data for detachment of particles from air bubbles[25,26,32]. In the case of flat fluid interfaces, qualitatively a similar behaviour is predicted theoretically[43–46,48,50,52] and also observed experimentally[44,46,47,52].

Figures 5, 6 and 7 show the dependence upon ν of the detachment force F^*, corresponding particle displacement Δr^*, and the Hookean ("spring") constant k, defined as

$$k = \left(\frac{dF}{d\Delta r} \right)_{\Delta r = 0}. \tag{51}$$

Note that the analytical formulas, derived in Section 5, in the limit of small particle-to-droplet size ratio, for the dependence of particle detachment position (Figure 6) and Hookean constant (Figure 7) work well even for relatively larger particles.

Next we consider different contact angles. The variation of the force with particle displacement, at different values of the contact angle θ, is shown in Figure 8. Figure 9 shows dependence of the detachment force as a function of contact angle, and Figure 10 displays the corresponding shapes of the droplet interface at the particle position corresponding to the maximum force.

Hysteresis of the contact angle may significantly affect the behaviour of the particles being detached from the interface[27,37,47]. Our model can still be applied in this case, if we take θ as the value of the receding contact angle.

5 Limit of small particles

In the most common cases the size of the particles is much smaller than the size of the droplet. This section focuses on investigating the limit of small particle to droplet size ratio.

5.1 General formulas.

In the small-particle limit the ratio of particle and droplet sizes ν, defined by Eq. (50) is a natural small parameter.

Since the radius of the contact circle cannot be larger than the radius of the particles, $\rho_c \leq a$, then this is always small compared to droplet size, too,

$$\rho_c \ll R. \tag{52}$$

The parameter ρ_0 is comparable with the size of the droplet,

$$\rho_0 \approx R. \tag{53}$$

The parameter c, which controls the deformation of the droplet, is also small in this limit:

$$c \ll 1. \tag{54}$$

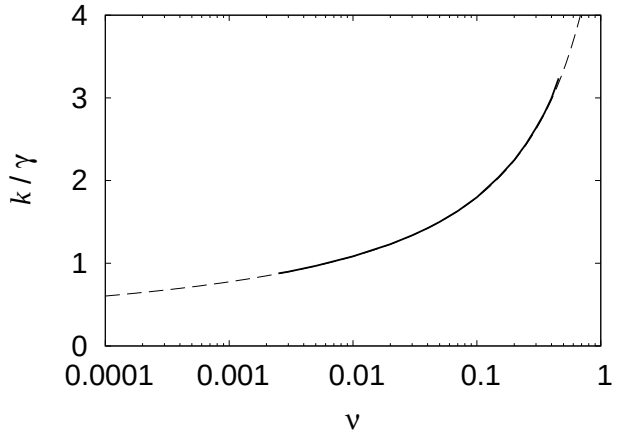

Fig. 7 Dependence of the Hookean constant defined by Eq. (51) upon ν at $\theta = 90^\circ$. Solid curve is calculated numerically. Dashed curve corresponds to the small-particle limit, Eq. (72).

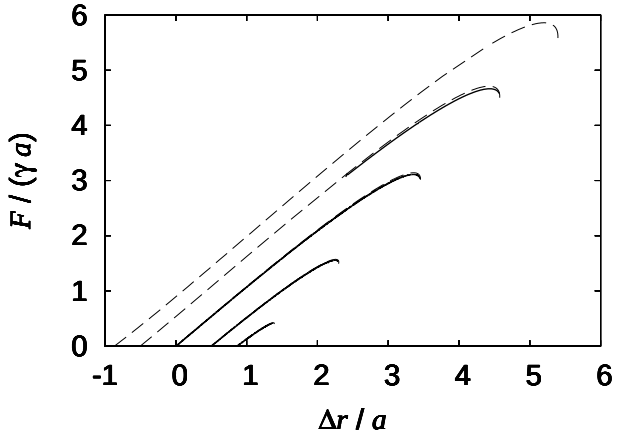

Fig. 8 Plots of force vs. the position of the particles, for $\nu = 0.01$. Solid curves are calculated numerically and correspond to $\theta = 150^\circ, 120^\circ, 90^\circ, 60^\circ, 30^\circ$ (from left to right). Dashed curves correspond to our analytical expression for the small-particle limit, Eqs (8) and (7). Note that the equilibrium position of the particles does not generally correspond to $\Delta r = 0$, except when $\theta = 90^\circ$.

This allows us to introduce the following set of dimensionless quantities:

$$\kappa \equiv \frac{\rho_c}{a}, \tag{55}$$

$$\lambda \equiv \frac{\rho_0 - R}{a}, \tag{56}$$

$$\mu \equiv \frac{c}{\nu}, \tag{57}$$

which in general are not small.

Let us choose κ as an independent parameter and regard μ, λ, as well as other quantities, as functions of κ. Then we can express the force given by Eq. (4) as a function of κ:

$$F(\kappa) = \frac{1}{2}\frac{(\partial \mathscr{F}/\partial \kappa)}{(\partial r/\partial \kappa)}. \tag{58}$$

In order to calculate the derivatives in Eq. (58), we need to express the free energy $\mathscr{F}$ and particle position r as functions of κ in small ν limit. For this we require the expressions for the parameters μ and λ as functions of κ.

The numerical solutions described in Section 4 have demonstrated that the actual contact angle at the surface of the particles in the absence of line tension remains equal to contact angle at flat surface, θ, as given by Young's equation, Eq. (3), with accuracy of the order 10^{-4}. This can be seen in Figure 12 where the top line is horizontal. To express μ in terms of κ, we will use this result from now on and fix the actual contact angle equal to θ expressed as

$$\theta = \arcsin\kappa - \arctan z'(\rho_c) \tag{59}$$

Substituting Eq. (24) for z' and expanding the result in powers of ν we obtain

$$\mu = 2\kappa\left(\sqrt{1-\kappa^2}\sin\theta - \kappa\cos\theta\right) + O(\nu). \tag{60}$$

To express λ in terms of κ we also expand the volume given by Eq. (47) in powers ν. Using the expansions of the elliptic integrals given by Eqs (91) and (92) (see Appendix), we obtain

$$V = \frac{4\pi R^3}{3}\left[1 + 3\left(\lambda - \frac{\mu}{4}\right)\nu + \frac{3}{16}\left(16\lambda^2 - 12\lambda\mu - \mu^2\right)\nu^2 + o\left(\nu^2\right)\right]. \tag{61}$$

The incompressibility condition, Eq. (6), then yields

$$\lambda = \frac{\mu}{4} + \frac{3\mu^2}{16}\nu + o\left(\nu^1\right), \tag{62}$$

Using the above expressions, we can write the free energy of the system in the following form:

$$\mathscr{F}(\kappa) = \mathscr{F}_0 - 2\pi a^2\gamma\left\{\kappa^2 + \frac{\mu^2}{4}\left[\frac{\xi}{\kappa+\xi} + \ln\frac{(\kappa+\xi)\nu}{4}\right] + 2\sqrt{1-\kappa^2}\cos\theta\right\} + o\left(\nu^0\right), \tag{63}$$

where

$$\mathscr{F}_0 = 4\pi R^2\gamma \tag{64}$$

is free energy of undeformed droplet without adsorbed particles, and ξ is defined by Eq. (9).

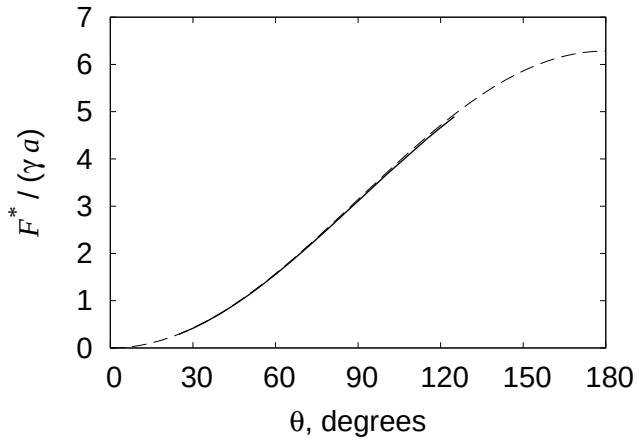

Fig. 9 Dependence of the detachment force upon contact angle at $v = 0.01$. Solid curve is calculated numerically. Dashed curve corresponds to the small-particle limit, Eq. (67).

In order to calculate force using Eq. (58), we also need the expression for the position of the particles, r, as a function of the parameter κ, too. Expressing r as

$$r = z(\rho_c) + \sqrt{a^2 - \rho_c^2}. \tag{65}$$

and expanding $z(\rho_c)$ given by Eq. (28) in v, we obtain

$$r(\kappa) = R + a\left\{\sqrt{1-\kappa^2} - \frac{\mu}{4}\left[1 + 2\ln\frac{(\kappa+\xi)v}{4}\right]\right\} + o\left(v^0\right), \tag{66}$$

which is equivalent to Eq. (8). Now substituting Eqs (63) and (66) into Eq. (58), we finally obtain Eq. (7) for the force.

Formulas (7) and (8), together with (9) and (10), allow us to calculate parametrically the dependence of the force F upon the position of the particles r in the small-particle limit (see Figure 8). The maximum force in the small-particle limit,

$$F^* = \pi\gamma a(1 - \cos\theta), \tag{67}$$

is shown in Figure 9. Note, the expression (67) coincides with the formula obtained by Scheludko *et al.*[41] for the case of flat fluid interface.

In our model we neglect compressibility of the inner fluid. Now we can demonstrate that this assumption is also valid in the case of gaseous bubbles. The change in free energy of the system due to the increase of the interfacial area, given by Eq. (63), is of order γa^2. The corresponding change in pressure is $\sim \gamma a^2/R^3$, where $V \sim R^3$ is the volume of the bubble. The inner fluid can be considered incompressible if this change is small compared to the Laplace pressure $\sim \gamma/R$. This yields the criterion $(a/R)^2 \ll 1$, which is well satisfied. Therefore, our formulas can be used for compressible (*eg.* air) bubbles as well.

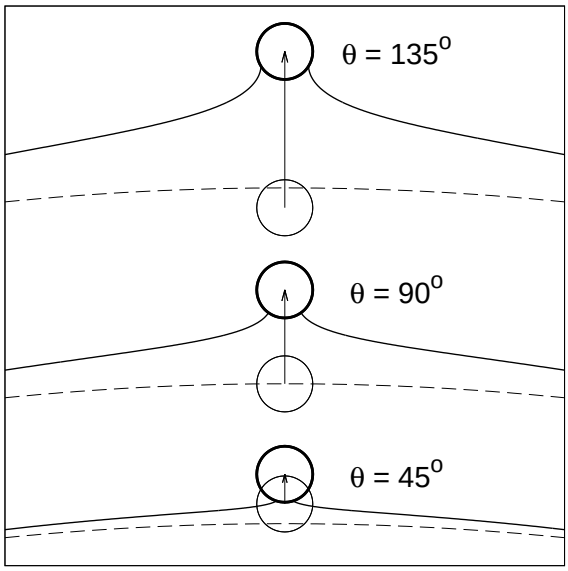

Fig. 10 Distortion of the shape of the droplet surface at particle positions corresponding to displacement where the maximum force occurs, for different contact angles. Results are calculated for $v = 0.01$. Dashed lines correspond to equilibrium shape of the droplet. Thin circles correspond to equilibrium positions of the particles (*i. e.* when $F = 0$).

5.2 Case of 90 degree contact angle.

For right angle contact angle ($\theta = 90°$) equations (8) and (7) simplify and the force and the position of the particles are given parametrically in terms of κ as follows:

$$F = 2\pi\gamma a\kappa\sqrt{1-\kappa^2}, \tag{68}$$

$$r = R + a\sqrt{1-\kappa^2}\left\{1 - \kappa\left[\frac{1}{2} + \ln\frac{\kappa(1+\kappa)v}{4}\right]\right\}. \tag{69}$$

From these formulas the dependence $\Delta r(F)$ can be obtained explicitly as Eq. (12). This variation is plotted in Figure 2. The maximum force

$$F^* = \pi\gamma a \tag{70}$$

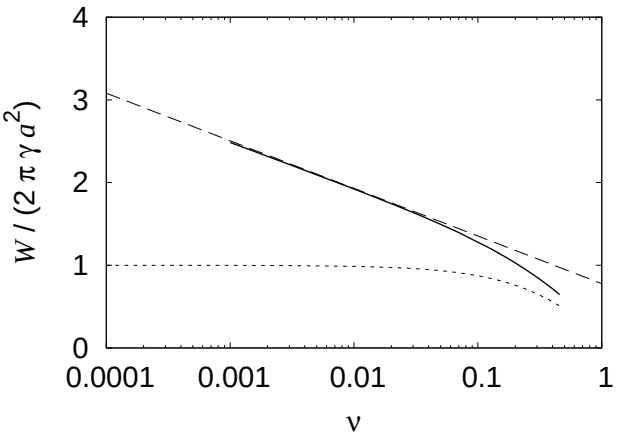

Fig. 11 Dependence of the detachment energy upon the value of ν for the case with $\theta = 90^\circ$. Solid curve is calculated numerically. Dashed curve corresponds to the small-particle limit, Eq. (74). Dotted curve shows the energy of adsorption for particle, included here for comparison.

occurs at position

$$r^* = R - \frac{a}{2}\left[\ln\frac{\left(\sqrt{2}+1\right)\nu}{8} - \sqrt{2} + \frac{1}{2}\right] \qquad (71)$$

(see Figure 6).

The Hookean constant defined by Eq. (51) is given by

$$k = \frac{2\pi\gamma}{\frac{1}{2} - \ln\frac{\nu}{2}} \qquad (72)$$

and is of the order of surface tension γ (see Figure 7). Numerical constants apart, the form of equation (72) is quite similar to that reported by Pitois and Chateau for k, obtained for the case of a flat interface in the limit of small Bond numbers[47]. However, it must be noted that the parameter ν for such problems is different to ours and there represents the ratio of the radius of the particle to the capillary length, $a/(\gamma/\rho g)^{1/2}$.

6 Work of detachment

As the two spherical particles are pulled gently apart, an increasing amount of energy is stored in the resulting distortion of the droplet (or bubble) surface. This situation continues until the displacement of the particles reaches a distance whereupon they become detached from the droplet. As already shown in Figure 2, the position at which this happens is slightly further away from the point where the generated restoring force attains its maximum value. At this stage, the interface relaxes back and the droplet returns to its original undisturbed spherical form, thus leaving the particles in the dispersion medium at a distance $\sim a$ away from the surface of the droplet. The process occurs over a finite relaxation time, dictated by the viscosities of the dispersed and the dispersion media. The localised flows of the fluid in the droplet and in that of the surrounding liquid close to the interfacially distorted region, taking place during this relaxation time, involve the dissipation of some of the stored interfacial energy. Typical stresses and strain rates involved in the process are γ/a and $\gamma/(\eta a)$, respectively, where for simplicity we assume that the viscosity, η, for the more viscous phase is much higher than the other one. The rate of energy dissipation per unit volume is then $\sim \gamma^2/(\eta a^2)$, i.e. inversely proportional to the viscosity. On the other hand, since the duration of the relaxation time increases linearly with η, it is expected that the overall dissipated energy during the full process should not be dependent on viscosity. The value of the energy dissipation, resulting from dislodging of the particles from the droplet surface, can be calculated by subtracting the stored energy in the distorted droplet interface just prior to particle detachment, from that of the particles that are fully displaced into the dispersed phase residing away from the droplet. The latter is simply given by Eq. (1), while the former is the area under the appropriate force–displacement curve, similar to those we displayed in Figures 2 and 8, integrated up to the point of detachment.

Figure 11 shows the dependence of the work required to detach the particles from the droplet on ν, calculated as

$$W = \mathscr{F}_{\text{detachment}} - \mathscr{F}_{\text{equilibrium}}. \qquad (73)$$

This work is compared with the adsorption energy, which is different from that given by Eq. (1) for flat interfaces due to deformation of the droplet in equilibrium.

As ν decreases, the dependence of the force upon the displacement of the particles becomes more linear. This allows calculating the detachment work, in small particle to droplet size ratio limit as the area of the triangle on the displacement–force diagram. Using Eqs (70) and (71) we can write for the case of the 90° contact angle:

$$W = -\frac{\pi}{2}\gamma a^2\left[\ln\frac{\left(\sqrt{2}+1\right)\nu}{8} - \sqrt{2} - \frac{1}{2}\right]. \qquad (74)$$

This is plotted in Figure 11, normalised by $2\pi\gamma a^2$. The dashed line in the figure is for our approximate equation, Eq. (74), while the solid line represents the exact results obtained using the numerical analysis of section 4.4. For values $\nu < 0.03$, the two curves are in perfect agreement, though they began to deviate at higher size ratios. The adsorption energy of the particles is also included in the figure, shown by the dotted line, for comparison. As expected, this is simply $2\pi\gamma a^2$ for the pair

of particles with a contact angle of 90°, when v is small. It marginally deviates from $2\pi\gamma a^2$ at higher size ratios, as the effects of the finite curvature of the interface become more prominent. Note that Eq. (74) provides the dissipated energy for the pair of particles and should be divided by a factor of two, if needed for a single particle. It is seen from Figure 11, that the dissipated energy becomes an increasingly more significant component of the work done during the detachment of the particles, in comparison to the adsorption energy, as $v \to 0$. The results in Figure 11 indicate that for small particles, the energy barrier to adsorption can be significantly larger than that simply taken to be equal to the adsorption energy. The detachment work of particles from the interfaces had also been considered by Pitois and Chateau[47] in the limit of small but finite Bond numbers (and therefore also flat interfaces). Their conclusions for such cases are broadly in accord with those found here.

Dissipation in moving the particle away from the surface is rate dependent but we are considering it post detachment only, assuming that up to the point of detachment the particle was moved sufficiently slowly so as to maintain the equilibrium liquid profile. Although in this case the exact energy dissipation during the detachment of the particle does not require any detailed knowledge of the of the actual relaxation dynamics, it maybe interesting to model this using LB or even traditional CFD methods. It would also be useful then to study the phenomenon using a high speed camera and compare the data with the theoretical results. To do so, it may be more suitable to use moderately viscous fluids, either for the droplet or the dispersion medium. This can easily be tailored to the appropriate value by adding a suitable amount of rheology modifiers or thickening agents to either of the two fluids, slowing down the interfacial relaxation kinetics to ranges that can easily be captured by the camera.

7 Effect of line tension

Line tension can affect the behaviour of the particles adsorbed at fluids interfaces if the particles are small enough[41,62–66],

$$a \sim \frac{\tau}{\gamma}. \tag{75}$$

Both positive and negative values of line tension τ were reported with magnitudes spanning a range $10^{-12} - 10^{-5}$ N.[63–65] Roughness of the contact line can also manifest itself as the effective line tension[67].

To account for line tension in our model, we add a contribution to the free energy of the system, Eq. (37), equal to the length of the contact circles of both particles multiplied by line tension:

$$\mathscr{F}_\tau = 4\pi\rho_c\tau. \tag{76}$$

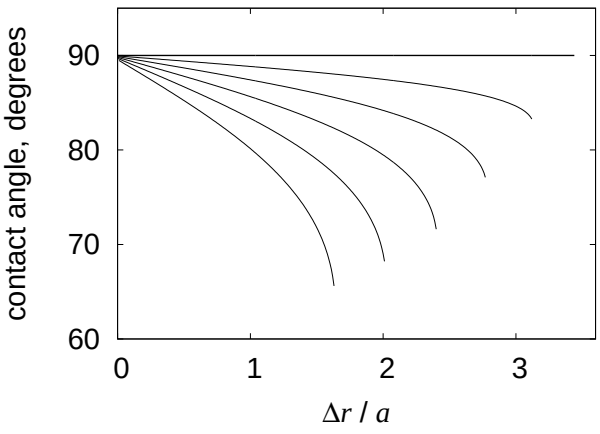

Fig. 12 Dependence of actual contact angle upon particles' positions at $v = 0.01$, $\theta = 90°$, and different values of dimensionless line tension $\tau/(\gamma a) = 0, 0.1, 0.2, 0.3, 0.4, 0.5$ (top to bottom).

Then we can minimise numerically the free energy of the system with the contribution of line tension given by Eq. (76) using the method described in Subsection 4.4.

Presence of line tension modifies the contact angle at the surface of the particles. Moreover, it makes it dependent upon the displacement of the particles, as is shown in Figure 12. This results in changes in the manner in which the force varies with displacement (Figure 13) and in the value of the detachment force (Figure 14). As expected[66], at large positive values of line tension the particles do not stay at the surface even in absence of any external force.

8 Conclusion

We have considered two spherical solid particles adsorbed on the surface of, and located at the opposite poles of an incompressible fluid droplet. We have calculated the deformation of the droplet and subsequent detachment of the particles under the influence of two opposite external forces applied to the particles at each end, as the magnitude of the forces is increased. The free-energy analysis have been used to calculate the force-displacement curves for restoring forces that are generated as a result of the droplet deformation and displacement of the particles relative to each other.

In the case of the particles being small compared to the droplet, the problem has been solved analytically. The force, given by Eq. (7), varies almost in a linear fashion with the displacement of the particle, Eq. (8), almost up to the point where the particle becomes detached from the droplet. The maximum force F^*, given by Eq. (67), depends upon the size of the particles a, the value of the surface tension γ, and the

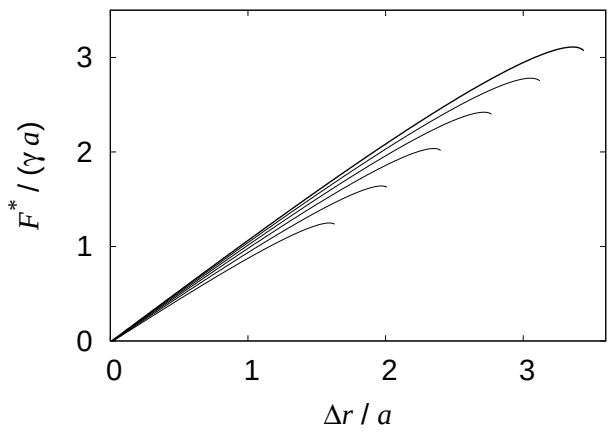

Fig. 13 Dependence of force on position of particles for cases where $\nu = 0.01$ and $\theta = 90^\circ$. Results are for different values of dimensionless line tension $\tau/(\gamma a) = 0, 0.1, 0.2, 0.3, 0.4, 0.5$ (from top to bottom).

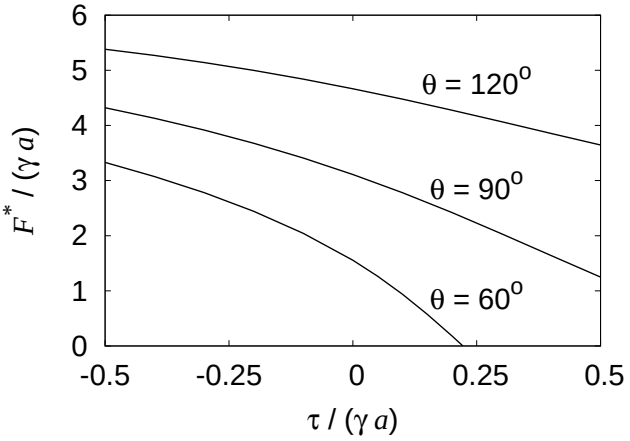

Fig. 14 Dependence of detachment force upon line tension at $\nu = 0.01$ and different values of the contact angle.

equilibrium contact angle θ in a way similar to that for a flat fluid interface. However, the dependence of the force upon the displacement of the particles is sensitive to the ratio of particle and droplet radii ν.

In the case of arbitrary ratio of particle and droplet radii, we have solved the problem "semi-analytically". These "exact" results agree with the analytical solution for small particles. At larger particle sizes the force decreases compared to the small-particle limit predictions, as shown in Figures 2 and 5. The effect of line tension becomes noticeable for particles of very small size given by Eq. (75).

The results of this work can be extended in several different directions. The series expansion in ν, derived in Section 5, can be extended by considering higher-order terms. This should result in better description of large particles. In particular, extended series should be able to describe the dependence of the detachment force upon ν, Figure 5. However, the formulas derived in Section 5 already have a good accuracy for the typical size ratios. For the dependence of particle detachment position (Figure 6) as well as Hookean constant (Figure 7) these formulas seem to work well even for larger particles.

Similar approach can be used to extend the results to the case of pinned contact line[68] and to particle shapes other than spherical. The work can be also extended to the case of surfactant-covered droplets by using Helfrich surface free energy[69]. The effect of adsorbed surfactant has been investigated experimentally by Spyridopoulos and Simons[28]. We expect that in such cases the global rather than local deformations of the droplet to play the main role due to curvature contribution to the free energy.

A Expansion of elliptic integrals

In this Appendix the series expansions of incomplete elliptic integrals $F(\varphi_c, k)$ and $E(\varphi_c, k)$ are derived for the small-particle limit described in Section 5.

In this limit the arguments of the elliptic integrals approach $\varphi_c \to \pi/2$ and $k \to 1$. Van de Vel[70] derived the series expansions of elliptic integrals valid in this double limit, which are summarised below.

The expansions are:

$$K(k) - F(\varphi, k) = \frac{2}{\pi} K(k') \sinh^{-1}\left(\frac{1}{k' \tan\varphi}\right) - \left(1 + k'^2 \tan^2\varphi\right)^{1/2} \cot^2\varphi \times \times \left(c'_0 - \frac{2}{3} c'_1 \cot^2\varphi + \frac{2\cdot 4}{3\cdot 5} c'_2 \cot^4\varphi - \ldots\right), \quad (77)$$

$$E(k) - E(\varphi, k) = \frac{2}{\pi}[K(k') - E(k')] \sinh^{-1}\left(\frac{1}{k' \tan\varphi}\right) + \left(1 - k^2 \sin^2\varphi\right)^{1/2} \cot\varphi - \left(1 + k'^2 \tan^2\varphi\right)^{1/2} \cot^2\varphi \times \left(d'_0 - \frac{2}{3} d'_1 \cot^2\varphi + \frac{2\cdot 4}{3\cdot 5} d'_2 \cot^4\varphi - \ldots\right). \quad (78)$$

In these formulas

$$k' = \sqrt{1 - k^2}, \quad (79)$$

$$c'_n = \frac{a'_n}{k'^{2n+2}} = \sum_{i=n+1}^{\infty} \binom{-\frac{1}{2}}{i}^2 k'^{2i-2n-2}, \quad (80)$$

$$d'_n = \frac{b'_n}{k'^{2n+2}} = \sum_{i=n+1}^{\infty} \binom{-\frac{1}{2}}{i}^2 \frac{2i}{2i-1} k'^{2i-2n-2}, \quad (81)$$

$$a'_n = \sum_{i=n+1}^{\infty} \binom{-\frac{1}{2}}{i}^2 k'^{2i}, \tag{82}$$

$$a'_0 = \frac{2}{\pi} K(k') - 1, \tag{83}$$

$$b'_n = \sum_{i=n+1}^{\infty} \binom{-\frac{1}{2}}{i}^2 \frac{2i}{2i-1} k'^{2i}, \tag{84}$$

$$b'_0 = \frac{2}{\pi} \left[K(k') - E(k') \right]. \tag{85}$$

and $\binom{n}{k}$ are binomial coefficients.

These formulas contain complete elliptic integrals of first and second kind, $K(k) = F(\frac{\pi}{2}, k)$ and $E(k) = E(\frac{\pi}{2}, k)$. For $|k| < 1$, they can be represented in terms of Gauss hypergeometric function ${}_2F_1(a,b;c;z)$ as follows[71]:

$$K(k) = \frac{\pi}{2} {}_2F_1\left(\frac{1}{2}, \frac{1}{2}; 1; k^2\right), \tag{86}$$

$$E(k) = \frac{\pi}{2} {}_2F_1\left(-\frac{1}{2}, \frac{1}{2}; 1; k^2\right). \tag{87}$$

Their asymptotic behaviour near the singularity at $k = 1$ is[71]

$$K(k) = \sum_{i=0}^{\infty} \left[\frac{\left(\frac{1}{2}\right)_i}{i!} k'^i \right]^2 \left[\ln\left(\frac{1}{k'}\right) + d(i) \right], \tag{88}$$

$$E(k) = 1 + \frac{1}{2} \sum_{i=0}^{\infty} \frac{\left(\frac{1}{2}\right)_i \left(\frac{3}{2}\right)_i}{(2)_i i!} k'^{2i+2} \times \\ \times \left[\ln\left(\frac{1}{k'}\right) + d(i) - \frac{1}{(2i+1)(2i+2)} \right], \tag{89}$$

where $(x)_n$ is Pochhammer symbol, and

$$d(x) = \psi(1+x) - \psi\left(\frac{1}{2} + x\right), \tag{90}$$

where $\psi(x)$ is digamma function.

Substituting the expressions (35) and (30) for φ_c and k in Eqs (77) and (78) we obtain the following formulas for the case of small ν:

$$F(\varphi_c, k) = -\ln \frac{(\kappa + \xi)\nu}{4} + o\left(\nu^0\right) \tag{91}$$

and

$$E(\varphi_c, k) = 1 - \left\{ \frac{\kappa^2}{2} + \frac{\mu^2}{16} \left[2 \ln \frac{(\kappa+\xi)\nu}{4} - \frac{\kappa - \xi}{\kappa + \xi} \right] \right\} \nu^2 \\ + o\left(\nu^2\right). \tag{92}$$

References

1 S. Ata, *Int. J. Mineral Processing*, 2012, **202**, 1–12.
2 S. Farrokhpay, *Adv. Coll. Int. Sci.*, 2011, **166**, 1–7.
3 R. J. Pugh, *Adv. Coll. Int. Sci.*, 1996, **64**, 67–142.
4 T. Tamura, M. Kageyama, Y. Kaneko and M. Nikaido, in *Emulsions, Foams, and Thin Films*, Marcel Dekker, New York, 2000, ch. Preparation of Novel Silicone-Based Antifoams Having a High Defoaming Performance, pp. 161–176.
5 B. P. Binks, *Curr. Opin. Coll. Int. Sci.*, 2002, **7**, 21–41.
6 E. Dickinson, *Curr. Opin. Coll. Int. Sci.*, 2010, **15**, 40–49.
7 S. Levine, B. D. Bowen and S. J. Partridge, *Coll. Surf.*, 1989, **38**, 325–343.
8 T. N. Hunter, R. J. Pugh, G. V. Franks and G. J. Jameson, *Adv. Coll. Int. Sci.*, 2008, **137**, 57–81.
9 B. S. Murray and R. Ettelaie, *Curr. Opin. Coll. Int. Sci.*, 2004, **9**, 314–320.
10 R. Aveyard, B. P. Binks and J. H. Clint, *Adv. Coll. Int. Sci.*, 2003, **100-102**, 503–546.
11 M. E. Cates and P. S. Clegg, *Soft Matter*, 2008, **4**, 2132–2138.
12 H. Firoozmand, B. S. Murray and E. Dickinson, *Langmuir*, 2009, **25**, 1300–1305.
13 M. N. Lee and A. Mohraz, *Adv. Mater.*, 2010, **22**, 4836–4841.
14 E. Kim, K. Stratford, R. Adhikari and M. E. Cates, *Langmuir*, 2008, **24**, 6549–6556.
15 K. Stratford, R. Adhikari, I. Pagonabarraga, J. C. Desplat and M. E. Cates, *Science*, 2005, **309**, 2198–2201.
16 K. Hwang, P. Singh and N. Aubry, *Electrophoresis*, 2010, **31**, 850–859.
17 E. Kim, K. Stratford and M. E. Cates, *Langmuir*, 2010, **26**, 7928–7936.
18 S. Melle, M. Lask and G. G. Fuller, *Langmuir*, 2005, **21**, 2158–2162.
19 J. W. Tavacoli, G. Katgert, E. G. Kim, M. E. Cates and P. S. Clegg, *Phys. Rev. Lett.*, 2012, **108**, 268306.
20 E. Bormashenko, *Curr. Op. Col. Int. Sci.*, 2011, **16**, 266–271.
21 G. McHale and M. I. Newton, *Soft Matter*, 2015, **11**, 2530–2546.
22 F. Sarvi, K. Jain, T. Arbatan, P. J. Verma, K. Hourigan, M. C. Thompson, W. Shen and P. P. Y. Chan, *Adv. Healthcare Mater.*, 2015, **4**, 77–86.
23 D. Zang, W. Zhang, J. Song, Z. Chen, Y. Zhang, X. Geng and F. Chen, *Appl. Phys. Lett.*, 2014, **105**, 231603.
24 H.-J. Butt, *J. Coll. Int. Sci.*, 1994, **166**, 109–117.
25 M. Preuss and H.-J. Butt, *J. Coll. Int. Sci.*, 1998, **208**, 468–477.
26 M. Preuss and H.-J. Butt, *Int. J. Miner. Process.*, 1999, **56**, 99–115.
27 S. Ecke, M. Preuss and H.-J. Butt, *J. Adhesion Sci. Technol.*, 1999, **13**, 1181–1191.
28 M. T. Spyridopoulos and S. J. R. Simons, *Trans. IChemE, Part A*, 2004, **82**, 490–498.
29 G. Gillies, K. Büscher, M. Preuss, M. Kappl, H.-J. Butt and K. Graf, *J. Phys. Condens. Matter*, 2005, **17**, S445–S464.
30 G. Gillies, M. Kappl and H.-J. Butt, *Adv. Coll. Int. Sci.*, 2005, **114-115**, 165–172.
31 D. J. Johnson, N. J. Miles and N. Hilal, *Adv. Coll. Int. Sci.*, 2006, **127**, 67–81.
32 J. Ally, M. Kappl, H.-J. Butt and A. Amirfazli, *Langmuir*, 2010, **26**, 18135–18143.
33 W. A. Ducker, Z. Xu and J. N. Israelachvili, *Langmuir*, 1994, **10**, 3279–3289.
34 H.-J. Butt, M. Kappl, H. Mueller and R. Raiteri, *Langmuir*, 1999, **15**, 2559–2565.
35 R. J. Hunter, *Foundation of Colloid Science*, Clarendon press, Oxford, 1987, vol. 1.
36 W. B. Russel, D. A. Saville and W. R. Schowalter, *Colloidal Dispersion*, Cambridge University press, Cambridge, 1989.
37 J. F. Joanny and P. G. de Gennes, *J. Chem. Phys.*, 1984, **81**, 552–562.
38 P. G. de Gennes, *Rev. Mod. Phys.*, 1985, **57**, 827–863.

39 C. W. Nutt, *Chem. Eng. Sci.*, 1960, **12**, 133–141.
40 A. D. Scheludko and A. D. Nikolov, *Coll. Polymer Sci.*, 1975, **253**, 396–403.
41 A. Scheludko, B. V. Toshev and D. T. Bojadjiev, *J. Chem. Soc. Faraday Trans. 1*, 1976, **72**, 2815–2828.
42 A. V. Rapacchietta, A. W. Neumann and S. N. Omenyi, *J. Coll. Int. Sci.*, 1977, **59**, 541–554.
43 A. V. Rapacchietta and A. W. Neumann, *J. Coll. Int. Sci.*, 1977, **59**, 555–567.
44 E. Bayramli, C. Huh and S. G. Mason, *Can. J. Chem.*, 1978, **56**, 818–823.
45 S. B. G. O'Brien, *J. Coll. Int. Sci.*, 1996, **183**, 51–56.
46 L. Zhang, L. Ren and S. Hartland, *J. Coll. Int. Sci.*, 1996, **180**, 493–503.
47 O. Pitois and X. Chateau, *Langmuir*, 2002, **18**, 9751–9756.
48 X. Chateau and O. Pitois, *J. Coll. Int. Sci.*, 2003, **259**, 346–353.
49 P. B. Kowalczuk and J. Drzymala, *Coll. Surf. A*, 2012, **393**, 81–85.
50 G. B. Davies, T. Krüger, P. V. Coveney and J. Harting, *J. Chem. Phys.*, 2014, **141**, 154902.
51 C. Huh and L. E. Scriven, *J. Coll. Int. Sci.*, 1969, **30**, 323–337.
52 C. Huh and S. G. Mason, *Can. J. Chem.*, 1976, **54**, 969–978.
53 R. Gunde, S. Hartland and R. Mäder, *J. Coll. Int. Sci.*, 1995, **176**, 17–30.
54 L. Zhang, L. Ren and S. Hartland, *J. Coll. Int. Sci.*, 1997, **192**, 306–318.
55 L. D. Landau and E. M. Lifshitz, *Fluid Mechanics*, Pergamon Press, Oxford, 1982.
56 G. B. Davies, T. Krüger, P. V. Coveney, J. Harting and F. Bresme, *Adv. Mater.*, 2014, **26**, 6715–6719.
57 J. Guzowski, M. Tasinkevych and S. Dietrich, *Eur. Phys. J. E*, 2010, **33**, 219–242.
58 F. M. Orr, L. E. Scriven and A. P. Rivas, *J. Fluid. Mech.*, 1975, **67**, 723–742.
59 O. Bolza, *Lectures on the calculus of variations*, University of Michigan Library, 2006.
60 J. Dinger, *Grundriss der Variationsrechnung*, F. Vieweg und Sohn, Braunschweig, 1867.
61 M. Hadzhilazova, I. M. Mladenov and J. Oprea, *Archivum Mathematicum (Brno)*, 2007, **43**, 417–429.
62 I. B. Ivanov, P. A. Kralchevsky and A. D. Nikolov, *J. Coll. Int. Sci.*, 1986, **112**, 97–107.
63 J. Drelich, *Coll. Surf. A*, 1996, **116**, 43–54.
64 J. Faraudo and F. Bresme, *J. Chem. Phys.*, 2003, **118**, 6518–6528.
65 A. Amirfazli and A. W. Neumann, *Adv. Coll. Int. Sci.*, 2004, **110**, 121–141.
66 B. Krasovitski and A. Marmur, *J. Adhesion*, 2005, **81**, 869–880.
67 A. I. Rusanov, *Mendeleev Comm.*, 1996, **6**, 30–31.
68 J. Ally, M. Kappl and H.-J. Butt, *Langmuir*, 2012, **28**, 11042–11047.
69 W. Helfrich, *Z. Naturforsch.*, 1973, **28c**, 693–703.
70 H. Van de Vel, *Math. Comp.*, 1969, **23**, 61–69.
71 *NIST Handbook of Mathematical Functions*, ed. F. W. J. Olver, D. W. Lozier, R. F. Boisvert and C. W. Clark, Cambridge University Press, 2010.